MARTIN MARIETTA ENERGY SYSTEMS LIBRARIES

3 4456 0283335 2

ORNL/TM-10428

ornl

OAK RIDGE NATIONAL LABORATORY

MARTIN MARIETTA

Consideration of the Magnetic Field Ripple in the Design of Plasma Edge Components for Tore Supra

C. C. Klepper
T. Uckan
P. K. Mioduszewski
R. T. McGrath
P. Hertout

OAK RIDGE NATIONAL LABORATORY
CENTRAL RESEARCH LIBRARY
CIRCULATION SECTION
4500N ROOM 175
LIBRARY LOAN COPY
DO NOT TRANSFER TO ANOTHER PERSON
If you wish someone else to see this report, send in name with report and the library will arrange a loan.

OPERATED BY
MARTIN MARIETTA ENERGY SYSTEMS, INC.
FOR THE UNITED STATES
DEPARTMENT OF ENERGY

Printed in the United States of America. Available from
National Technical Information Service
U.S. Department of Commerce
5285 Port Royal Road, Springfield, Virginia 22161
NTIS price codes—Printed Copy: A03; Microfiche A01

This report was prepared as an account of work sponsored by an agency of the United States Government. Neither the United States Government nor any agency thereof, nor any of their employees, makes any warranty, express or implied, or assumes any legal liability or responsibility for the accuracy, completeness, or usefulness of any information, apparatus, product, or process disclosed, or represents that its use would not infringe privately owned rights. Reference herein to any specific commercial product, process, or service by trade name, trademark, manufacturer, or otherwise, does not necessarily constitute or imply its endorsement, recommendation, or favoring by the United States Government or any agency thereof. The views and opinions of authors expressed herein do not necessarily state or reflect those of the United States Government or any agency thereof.

ORNL/TM-10428
Dist. Category UC-421,424,426

Fusion Energy Division

CONSIDERATION OF THE MAGNETIC FIELD RIPPLE IN THE DESIGN OF PLASMA EDGE COMPONENTS FOR TORE SUPRA

C. C. Klepper
T. Uckan
P. K. Mioduszewski
R. T. McGrath[a]
P. Hertout[b]

Date published: October 1988

[a]Sandia National Laboratories, Albuquerque, New Mexico 87175
[b]Centre d'Etudes Nucléaires, Cadarache, France

Prepared by the
OAK RIDGE NATIONAL LABORATORY
Oak Ridge, Tennessee 37831
operated by
MARTIN MARIETTA ENERGY SYSTEMS, INC.
for the
U.S. DEPARTMENT OF ENERGY
under contract DE-AC05-84OR21400

MARTIN MARIETTA ENERGY SYSTEMS LIBRARIES
3 4456 0283335 2

CONTENTS

ABSTRACT v

I. INTRODUCTION 1

II. THE TORE SUPRA TOKAMAK 2

II.A. Pump Limiters 2

II.B. RF Antennas 2

III. MAGNETIC FIELD MODEL 3

III.A. Field Line Tracing 6

III.B. Poloidal and Vertical Fields 7

III.C. Application to the Outboard Limiter Module 8

III.C.1. Effect on Particle Removal 11

III.C.2. Effect on Heat Handling 11

III.C.3. Reshaping of the Limiter Head 12

III.C.4. Sensitivity to Limiter Radius 14

III.D. Application to RF Antennas 16

IV. ANALYTICAL MODEL 16

V. CONCLUSIONS 19

ACKNOWLEDGMENTS 20

REFERENCES 21

ABSTRACT

Design of edge components for a plasma device requires a description of heat and particle flows at the edge of the device. In a tokamak, the ripple of the toroidal field affects the direction of such flows by affecting the direction of the field. In Tore Supra, in particular, the ripple is large ($\leq$8% at the outboard edge). This causes a substantial ($\leq$ factor of 2) increase in heat flux deposited onto the limiter and antenna face. It also reduces the particle removal efficiency of the pump limiters by increasing the distance between the throat opening and the plasma edge. It is therefore important to include the ripple when designing plasma edge components such as pump limiters and rf antennas. A simple, but accurate, scheme for field line tracing is found and used to study this effect. Modeling of the ripple is discussed.

I. INTRODUCTION

In the design of components that come into contact with the plasma at the edge of a tokamak, the effects of high heat flux at the surface of these devices must be considered. Such components include limiters, divertor plates, and radio frequency (rf) antennas. Often, to optimize their heat removal capability, the components are shaped so that they are nearly parallel to the direction of the flux near the plasma edge, where the heat flux is highest, and become more perpendicular as the distance between the surface of the device and the plasma edge increases. Typically, the heat flux decays exponentially with distance from the plasma edge. In this way, the normal component of heat flux can be made nearly constant over the surface. Its upper limit is dictated by technology. Operation of edge components near such limits causes even small errors in the shaping of their surfaces to be detrimental.

Because the ripple of the magnetic field (Fig. 1) affects the direction of the particles and, therefore, heat flow at the edge of a tokamak, the ripple should be taken into account in the design of such surfaces. Furthermore, in a pump limiter module, ripple in the edge field lines will affect the distance between the opening of the throat of the module and the edge of the plasma, leading to decreased particle trapping. Also, charged particles trapped in the throat are still guided by

ORNL-DWG 86-2991 FED

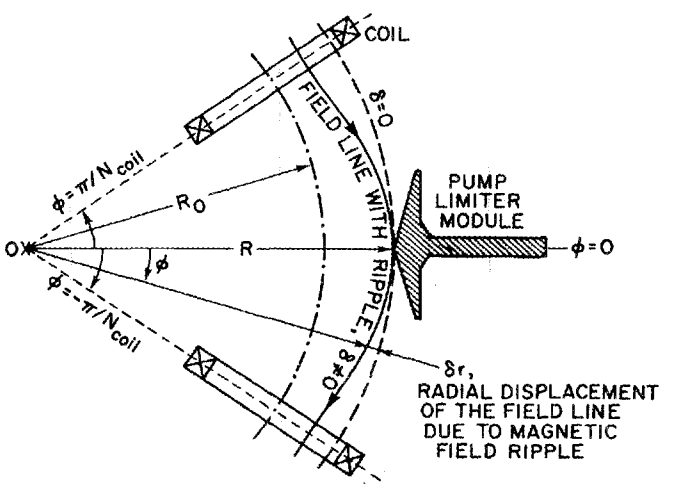

Fig. 1. Magnetic field ripple.

the magnetic field to the neutralizer plate, where they are reflected or recycled as neutrals. The ripple in the field will affect the path of these particles, possibly causing them to miss the neutralizer.

The amplitude of the ripple, δ, is defined as

$$\delta = \frac{B_{\max} - B_{\min}}{B_{\max} + B_{\min}} ,$$

where $B_{\max}$ and $B_{\min}$ are the maximum and minimum values of the field at a given radius and poloidal angle. In Tore Supra, δ is as large as 6.5–8.3% at the outer midplane, depending on limiter radius. This is an unusually large ripple and must be considered in the design of the edge components. The effect of the ripple on particle transport is not considered in this paper. It has been studied by other authors both for Tore Supra[1] and for other machines.[2–5]

II. THE TORE SUPRA TOKAMAK

Tore Supra is a large (R_0 = 238 cm, a = 80 cm), long-pulse ($\leq$30 s), high-input-power ($\leq$15 MW) tokamak that features superconducting toroidal field (TF) coils.[6]

II.A. Pump Limiters

Seven pump limiter modules will be used in Tore Supra for particle control. One of the modules will be installed at the outboard midplane; the others will be placed on the top and bottom of the torus. The dimensions of the heads of these modules are approximately 50 by 50 cm for the outboard and 40 by 40 cm for the top/bottom modules. The outboard limiter module is designed to remove 2 MW of the power flowing to the edge of the device. The vertical modules are designed to handle 1 MW each. To handle such heat loads for the duration of the long Tore Supra discharges, the modules will be made entirely of cooling channels imbedded in graphite armors. Modeling of these limiter modules' heat and particle removal capabilities is found elsewhere.[7]

II.B. RF Antennas

The three rf antennas planned for Tore Supra will be located at the outboard midplane. Their dimensions are about the same as those of the outboard pump limiter module. Because the antennas will be placed in the shadow of the limiters,

the heat handling requirements are more relaxed for the antennas than for the limiter modules. Particle removal is not relevant. What is important is whether the electron density at the Faraday shield of the antenna is high enough to permit proper coupling.

III. MAGNETIC FIELD MODEL

One of the requirements for proper computation of the effect of ripple on an edge component is the ability to trace field lines in space from any point on the surface. This allows for calculation of both the change in the angle of incidence of the heat flux on the surface and the change in distance between the component and the plasma boundary, which has the shape of the last closed field line at the location of the edge component.

Tokamak TF models found in the literature typically pertain to noncircular TF coils.[3,4,8,9] In these models, the TF coils are modeled by loops, each composed of a small number of straight filaments. For studies that require computation of the field near (or even inside) the coil, models that use discrete loops must be replaced by more elaborate models that use an appropriate, continuous-current distribution within the coil cross section.[10]

In the case of Tore Supra, the TF coils are circular. This allows for simpler models that approximate each TF coil by a set of circular loops. Computer codes that model the Tore Supra TF coils by using a large number of loops to achieve a nearly constant current density (CCD) already exist.[11,12] Such computations are time consuming and therefore inappropriate for repetitive use. For this study, a model was developed in which each of the 18 TF coils is approximated by a set of only five current-carrying circular loops. The locations of the loops within the physical extent of the coil and the distribution of the total current between these loops are adjusted until the results agree, to better than 10%, with those of the CCD model, which were available for a few points. Figure 2 shows the distributions of the loops and of the current among the loops that produce this agreement in the vacuum fields. Note that this replacement of a CCD model by one that uses a few discrete loops is feasible here only because the largest minor radius of interest is less than 70% of the radius of the coil.

The elliptic integral equations that describe the components of the magnetic field caused by a current-carrying, circular loop can be found in the literature.[13] For this

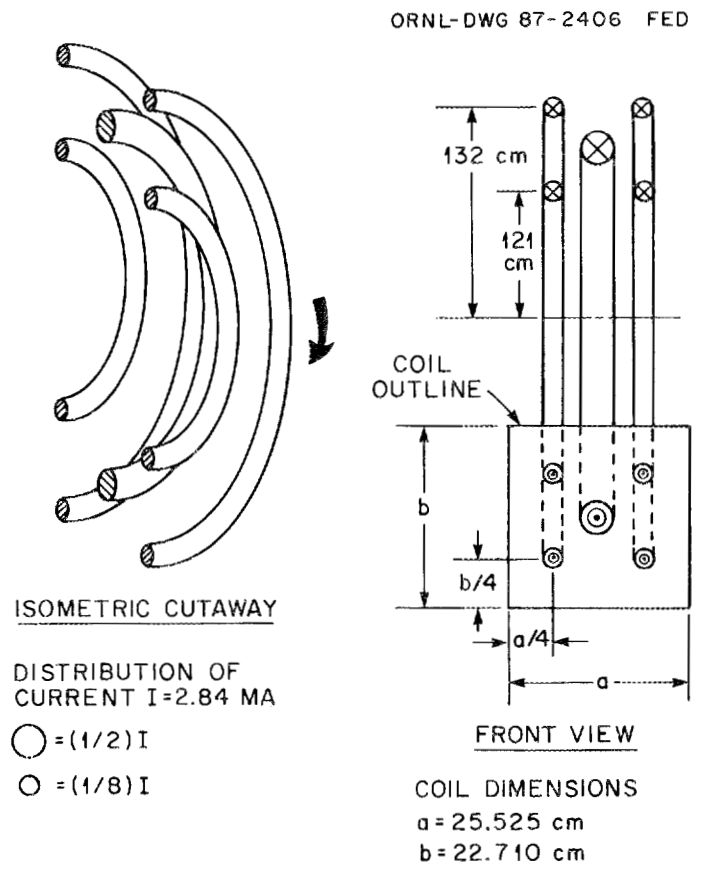

Fig. 2. Optimal distribution of five current loops and of the total current in each of 18 Tore Supra toroidal field coils to approximate CCD.

calculation, a computer code called BDLOOP[14] was used. The code computes and sums the components of the field that results from an arbitrary number of loops, arbitrarily placed and oriented in space. The loops were placed in the following manner.

Let r_0, r_1, and r_2 be the radii of the three types of current loops in each coil. First, 18 loops of radius r_0 are placed such that their centers are at a radial distance $R_0 = 244.3$ cm from the axis of the torus and their toroidal angle increments are $\Delta\phi = 2\pi/N_{\text{coil}}$, where $N_{\text{coil}} = 18$ (the number of coils).

The orientation of each loop is determined by the angles θ and ϕ of the axis of the loop in the r, θ, ϕ coordinate system centered on the center of the loop. For this first set of loops,

$$\cos\phi = \cos\left(\Phi + \frac{\pi}{2}\right) \quad ,$$

$$\sin\phi = \sin\left(\Phi + \frac{\pi}{2}\right) \quad ,$$
$$\sin\theta = -1 \quad ,$$
$$\cos\theta = 0 \quad ,$$

where Φ is the toroidal angle of the center of the loop. The loop radius, $r_0 = 1.2668$ m, is the same as the mean radius of the coil.

The second set of loops is placed at the same major radius, but with a toroidal shift $\delta\Phi = 0.0261$ rad (or 1.5°; the actual coil spans 3° on each side of its midplane). The loop radius for this set is $r_1 = 1.3235$ m $> r_0$. This is the midpoint between the mean radius and the outer radius of the coil.

Note that the loops must be parallel to each other. To accomplish this, the orientation of the loop is determined from the toroidal angle of the coil midplane. That is, if Φ is the toroidal angle of the loop and Φ_0 is that of the midplane, the loop is placed at

$$\cos\phi = \cos\left(\Phi_0 + \frac{\pi}{2}\right) \quad ,$$
$$\sin\phi = \sin\left(\Phi_0 + \frac{\pi}{2}\right) \quad ,$$
$$\sin\theta = -1 \quad ,$$
$$\cos\theta = 0 \quad .$$

Similarly, a third set of 18 loops has a toroidal shift $\delta\Phi = -0.0261$ rad with respect to the coil midplane and has the same loop radius as the second set.

The fourth and fifth sets are placed like the second and third, but they have a smaller radius $r_2 = 1.2100$ m $< r_0$, such that $(r_1 + r_2)/2 = r_0$.

Optimal results (best agreement with the vacuum field) are achieved for this configuration when the central loop in each coil carries half of the total coil current,

$$I_0 = \frac{1}{2}\, I_{\rm coil} = \frac{1}{2}\,(2.84 \text{ MA}) \ ,$$

and each of the other four loops carries

$$I_1 = \frac{1}{8}\, I_{\rm coil} = \frac{1}{8}\,(2.84 \text{ MA}) \ .$$

With this configuration of current loops, the values computed for amplitude of the ripple, δ, at the outboard and top/bottom locations for plasma $R_0 = 238$ cm and $a = 80$ cm are 7.95% and 3.89%, respectively. The ratio of these values is $\delta_{\rm out}/\delta_{\rm top} = 7.95/3.89 = 2$.

This ratio was found to be almost independent of the placement of the loops within each coil and of the distribution of current. However, values of the ripple amplitude δ are very sensitive to such distributions. The CCD computation gives values of 8.35% and 3.81%, respectively, for the outboard and top/bottom ripple strengths. The ratio is 2.19. The largest deviation of the five-loop simulation from these values is about 5%.

III.A. Field Line Tracing

Once it is possible to obtain the components of the field for any location within the torus, a field line can be traced by using the magnetic field line equation

$$dR/B_R = Rd\Phi/B_\Phi = dZ/B_Z \quad .$$

Figure 3 shows a field line traced from the tangency point of the outboard limiter assumed at $R_0 + a = 236 + 75$ cm over a toroidal extent of 10° (the separation of the coils is 20°). A trace of the same field line by means of the CCD calculation is superimposed in Fig. 3. The toroidal extent of interest for the edge components is about 5°. The noticeable deviation of the five-loop model from the CCD model (~10%) occurs near the coil and is caused by the approximation of the CCD by discrete current loops.

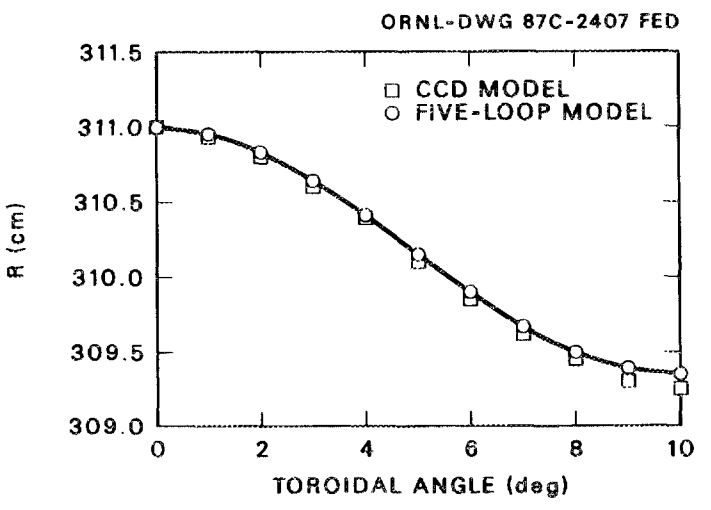

Fig. 3. Comparison of field lines traced by five-loop-per-coil simulation and by CCD computation. Data are for a field line at $R = 311$ cm.

III.B. Poloidal and Vertical Fields

Thus far, only vacuum fields have been considered. To complete the simulation, a current loop is added, this time on the midplane of the torus; that is,

$$\cos\phi = 1 \quad ,$$

$$\sin\phi = 0 \quad ,$$

$$\cos\theta = 1 \quad ,$$

$$\sin\theta = 0 \quad ,$$

It carries a current of 1.7 MA, simulating the plasma current. The loop radius is chosen as

$$r_c = R_0 + \Delta_{\rm sh} \quad ,$$

where

$$\Delta_{\rm sh} = \frac{a^2}{2R_0}\left(\beta_p + \frac{l_i}{2} - \frac{1}{2}\right)$$

is the Shafranov shift. Values for β_p and $l_i/2$ for Tore Supra are $\sim$1 and $\sim$1/2, respectively.

The placement of such a shifted current loop results in a significant Z component of the field in the top/bottom locations. This must be canceled by means of a vertical field computed as[15,16]

$$B_Z = \frac{\mu_0 I_P}{4\pi R_0}\left(\ln\frac{8R_0}{a} + \beta_p + \frac{l_i}{2} - \frac{3}{2}\right) \quad .$$

For this case, $B_Z = 0.226$ T.

As a check, the resulting poloidal field is compared with that predicted by the Shafranov poloidal field equation:

$$B_\theta = -\frac{\mu_0 I_P}{2\pi a}\left[1 + \frac{a}{R_0}\cos\theta\left(\beta_p + \frac{l_i}{2} - 1\right)\right] \quad ,$$

which shows good agreement.

The contribution of the poloidal and vertical fields to the effect of ripple on the edge components was found to be negligible. This can be attributed to the fact that, for a plasma safety factor $q \approx 3$, a field line moves poloidally a distance of only about 1% of the total poloidal circumference over the typical toroidal extent of the component. The field line does not sample a significant change in the amplitude of the ripple. It is therefore sufficient to consider only the vacuum field lines.

III.C. Application to the Outboard Limiter Module

The capability of tracing field lines from each point on the surface of the limiter head makes it possible to compute the distances of each point along the front surface of the outboard pump limiter module from the plasma edge. The shape of the pump limiter head, designed on the basis of an assumption of nonrippled edge field lines, is shown in Fig. 4a.[17] The vacuum field lines shown in this figure are circles. The unrippled field line contacting the tangency point of the limiter (i.e., the point closest to the plasma) is a circle of radius 312.5 cm ($R_0 = 237.0$ cm, $a = 75.5$ cm). The remaining field lines shown in the figure have a radius progressively incremented by 1 cm. The figure, which shows the front surface, the neutralizer plate, and a sketch of the shelf, is essentially a cross section of the outboard limiter head in the Tore Supra midplane. In this cross section, the front surface consists of two joining straight-line segments of different slope, followed by a circular leading edge. Only half of this cross section is displayed, because of symmetry. This shape was chosen for its simplicity and also because it distributes the heat flux along the front face in a manner consistent with the heat removal capabilities of the embedded cooling channels (not shown in the figure). This shape also allows for a minimum distance of the throat opening from the edge while keeping the maximum heat flux density at the leading edge below the 3-kW/cm^2 limit imposed by the technology.

Notice that, at the leading edge, the throat opening is about 2.5 cm from the plasma edge, which is defined by the field line tangent to the limiter at $x = 0$. Also, most of the field lines entering the throat actually reach the neutralizer. In Fig. 4b, the distance, Δy, of each point along the toroidal extent of the limiter front surface from the plasma edge and the angle, θ, between the field lines (also particle and heat fluxes) and the surface at each point are plotted. From these, the heat flux density Q at each toroidal location is computed as

$$Q = Q_0 e^{-\Delta y/\lambda_Q} \sin\theta \ ,$$

where λ_Q is the heat flux scrape-off length, and is also plotted in the figure. The edge parallel heat flux Q_0 is adjusted so that the total power handled by the limiter is 2 MW. The assumed poloidal extent is 53 cm.

Figures 5a and 5b show the same quantities for rippled field lines. From Fig. 5a, it is evident that the particle removal efficiency is greatly reduced because of two resulting effects. First, the throat opening is moved away from the plasma by about an additional 1 cm. Second, the neutralizer is largely shadowed by the limiter head.

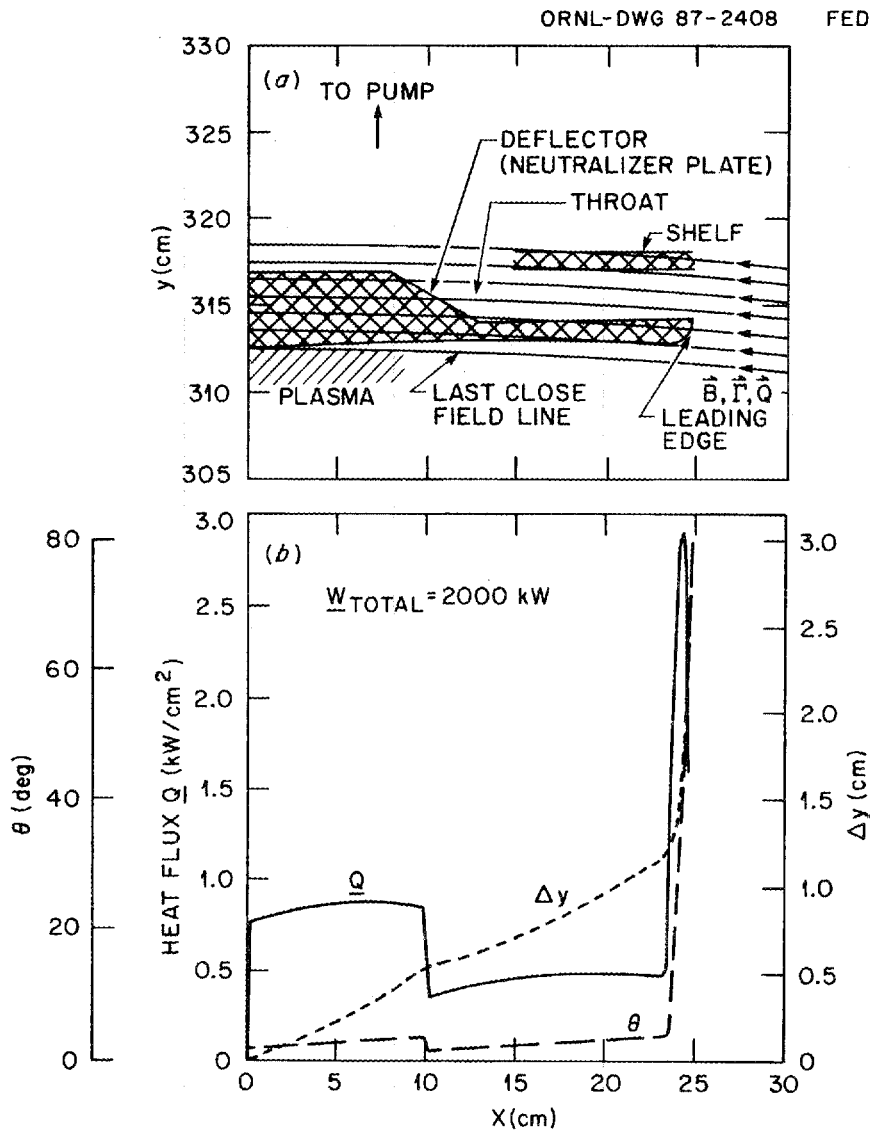

Fig. 4. Plots for the unmodified limiter head and the nonrippled (circular) field lines for which it was designed: (a) a graph showing the front surface of the head and edge field lines, including a sketch of the shelf and neutralizer; and (b) a graph showing distances (Δy) between the front limiter surface and the plasma edge as a function of x (measured along the tangent to the plasma edge at the plasma-limiter tangency point), the angle (θ) between the field lines and the surface, and heat flux density (Q) on the surface that has been normalized so that the total power removed from the limiter is 2 MW.

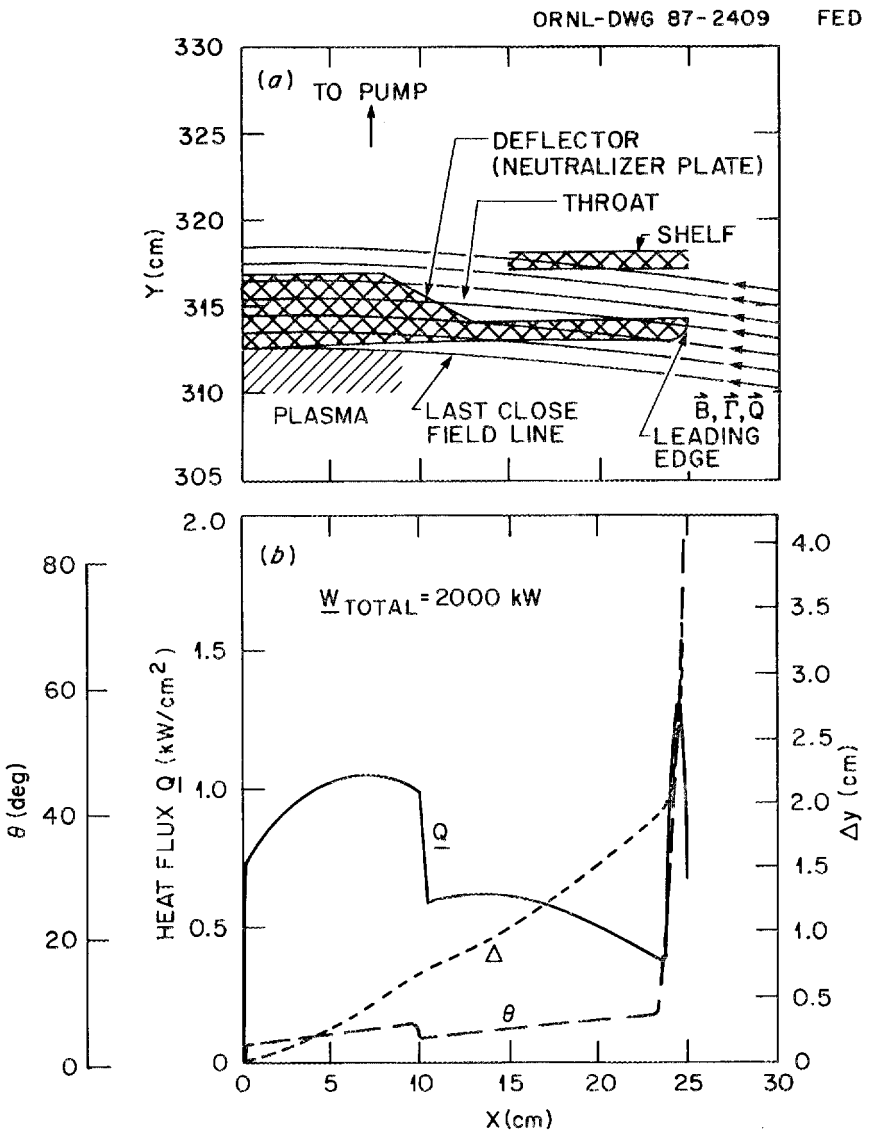

Fig. 5. Plots for the unmodified pump limiter head and rippled field lines: (a) a graph showing the front surface of the head and edge field lines and (b) a graph showing distances (Δy) between the front limiter surface and the plasma edge, the angle (θ) between the field lines and the surface, and the heat flux density (Q) on the surface that has been normalized so that the total power removed from the limiter is 2 MW.

Figure 5b shows that the heat handled by the front face of the limiter is increased whereas the heat handled by the leading edge is decreased, as compared with the designed values (as determined from Fig. 4b).

III.C.1. Effect on Particle Removal

The loss in particle removal efficiency can be estimated as follows. The efficiency depends on the head thickness x_h of the limiter as

$$\epsilon \sim e^{-x_h/\lambda_\Gamma}(1 - e^{-\Delta/\lambda_\Gamma}) \quad ,$$

where Δ is the throat width and λ_Γ is the particle flux scale length. The effect of the ripple is to increase x_h by about 0.8 cm at the limiter radius of interest. This, as may be observed qualitatively in Fig. 5a, is caused by the fact that the last closed field line, which describes the plasma edge, shifts radially inward as it moves from the tangency point toward the leading edge.

The decrease in efficiency is then obtained by comparing the efficiency with no ripple to that with ripple:

$$\epsilon_{\rm NR} \sim e^{-2.5/3.0}(1 - e^{-3.0/3.0}) = 0.53 \quad ,$$

(assuming $\lambda_\Gamma \approx \lambda_n \approx 3$ cm), while

$$\epsilon_{\rm R} \sim e^{-3.3/3.0}(1 - e^{-3.0/3.0}) = 0.21 \quad ,$$

resulting in

$$\epsilon_{\rm NR} - \epsilon_R = \frac{0.53 - 0.21}{0.53} = 60\% \text{ decrease} \quad .$$

However, as mentioned in the introduction, there is an additional effect—shadowing of the neutralizer plate by the limiter head. Figure 5a shows how it can be estimated that 50% of the neutralizer is shadowed. This means that the width of the throat, Δ, is reduced by a factor of 2 to about 1.5 cm. That reduction changes $\epsilon_{\rm R}$ from 0.21 to 0.14, leading to a 73% (instead of 60%) decrease in exhaust efficiency.

III.C.2. Effect on Heat Handling

As for the heat handling capabilities of the limiter, a comparison of Figs. 4b and 5b shows an increase of about 17% in the (integrated) heat load handled by the front face of the module. The change in heat flux at each point along the

front face is shown in Fig. 6. The maximum increase in heat flux on the front face occurs at about 10 cm and is 68%. This value approaches 100% as the maximum outboard limiter radius of $R_{L} = 318$ cm is approached, where the amplitude of the ripple is about 8%. The location of this maximum is determined by a competition between two effects: (a) the increasing radial component of the field as the toroidal angle increases from the tangency point to the midpoint between the tangency point and the nearest coil and (b) the decrease in heat flux as the distance between the surface and the plasma edge increases. Also, the leading edge, which was designed to handle up to 3 kW/cm^2, actually handles only half that value. The penalty is in the reduced particle exhaust, as discussed earlier.

III.C.3. Reshaping of the Limiter Head

To compensate for the effect of ripple, each of a large number of points along the toroidal extent of the limiter is shifted in the y direction by an amount obtained by subtracting the values of Δy in Fig. 4b from those in Fig. 5b. The resulting surface is then compensated for particle removal efficiency, as seen in Fig. 7a, and

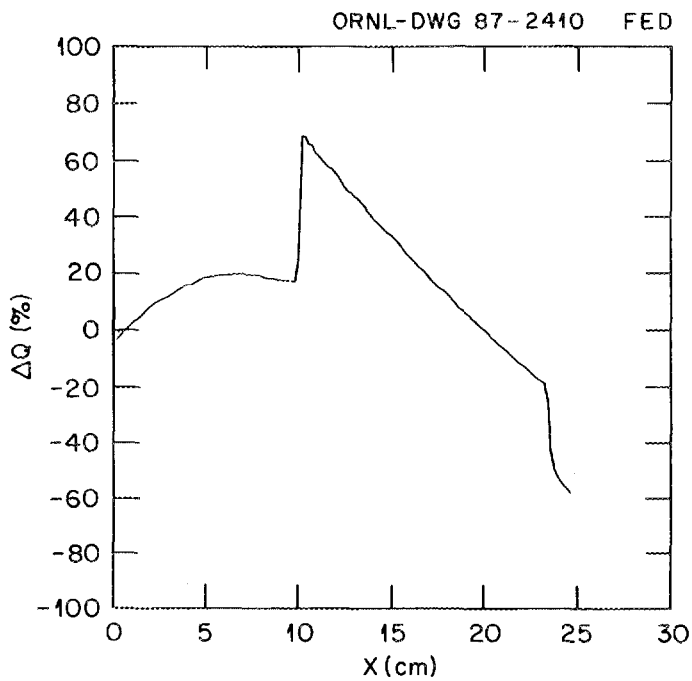

Fig. 6. Changes in the heat flux normal to the pump limiter surface caused by ripple.

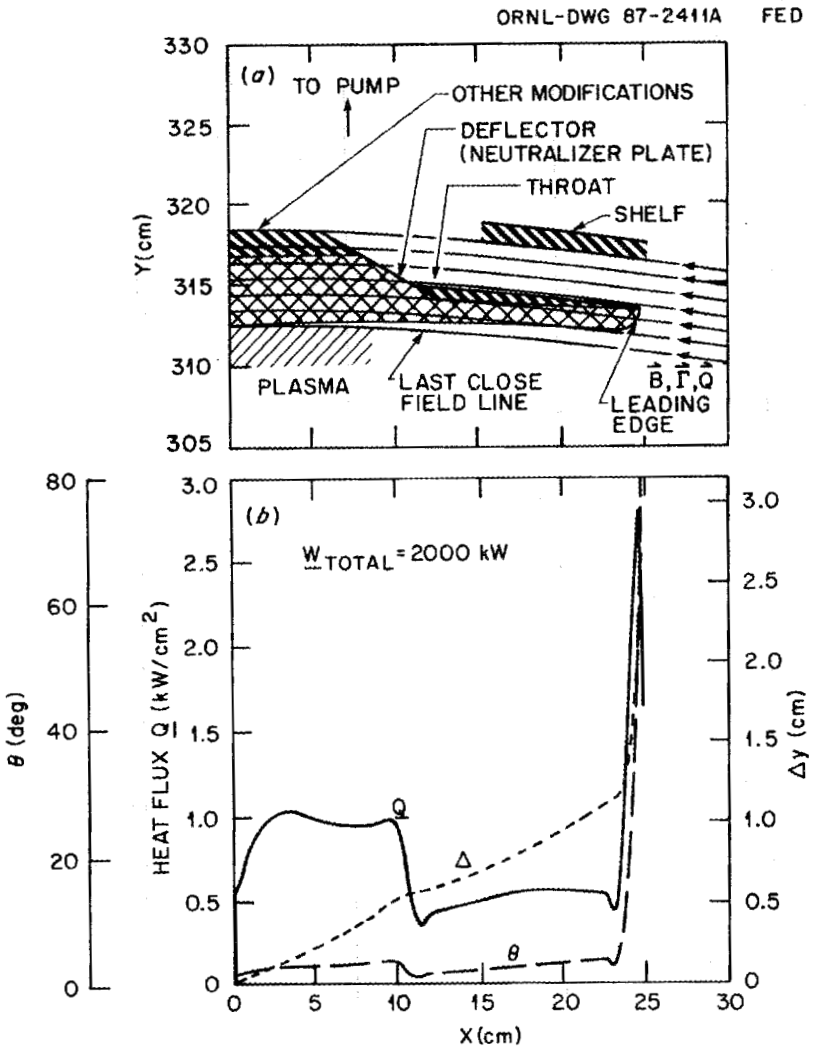

Fig. 7. Plots for the modified pump limiter head and rippled field lines: (a) a graph showing the front surface of the head and edge field lines and (b) a graph showing distances (Δy) between the front limiter surface and the plasma edge, the angle (θ) between the field lines and the surface, and the heat flux density (Q) on the surface that has been normalized so that the total power removed from the limiter is 2 MW.

presumably for heat handling; the latter is checked in Fig. 7b. Because the shifts are made at discrete points, a certain amount of interpolation and smoothing was used to produce the slopes of the surface at these points. This resulted in the smooth curve seen in Fig. 7b.

As mentioned earlier, the shifts in y as a function of x were computed by subtracting the Δy values computed with and without ripple. Actually, to produce the shape of Fig. 7, the shifts were performed as computed only for the flat sections of the limiter. The circular leading edge was shifted as a single unit. The neutralizer and the shelf were not changed in this exercise, but they should be corrected in the final design.

III.C.4. Sensitivity to Limiter Radius

The limiter was shaped according to the edge field line traces at the reference limiter location, which is $R_{\rm lim} = 312.5$ cm (i.e., $R_0 = 237$ cm and $a = 75.5$ cm). The problem is that this is a movable limiter, and it may be necessary to operate it at a different radial location. One example of such operation is that of $R_{\rm lim} = 307$ cm, which would put the plasma in contact with the inner wall. This would be done if the limiters could not handle the power lost to the edge without some power sharing with the inner (cooled) wall. An outward shift of the limiter to $R_{\rm lim} = 317$ cm would also allow the plasma to contact the inner wall, by also allowing the plasma to expand to an 80-cm minor radius.

Figures 8a through 8d show how limiter performance is affected by these changes in radial location. Figure 8a shows that the exhaust efficiency of the outboard limiter module increases by about 10% from its reference value when the module is moved inward. The ripple amplitude is decreased and the shape of the limiter head overcompensates for the ripple. The leading edge is now closer to the plasma edge than allowed, and the resulting penalty is a higher heat flux, as seen in Fig. 8b. This calculation assumes that the outer limiter always handles a total power of 2 MW (as designed). However, at the larger limiter radius of 317 cm, the exhaust efficiency is somewhat reduced compared with the reference value and so is the heat flux at the leading edge. This computation neglects small changes in the shadowing of the neutralizer by the head of the module.

Figure 8c shows the effect of changing the limiter radius on the total power handled by the front face of the limiter (excluding the leading edge). As the limiter moves outside, the worsening ripple causes a larger radial heat flux, which increases

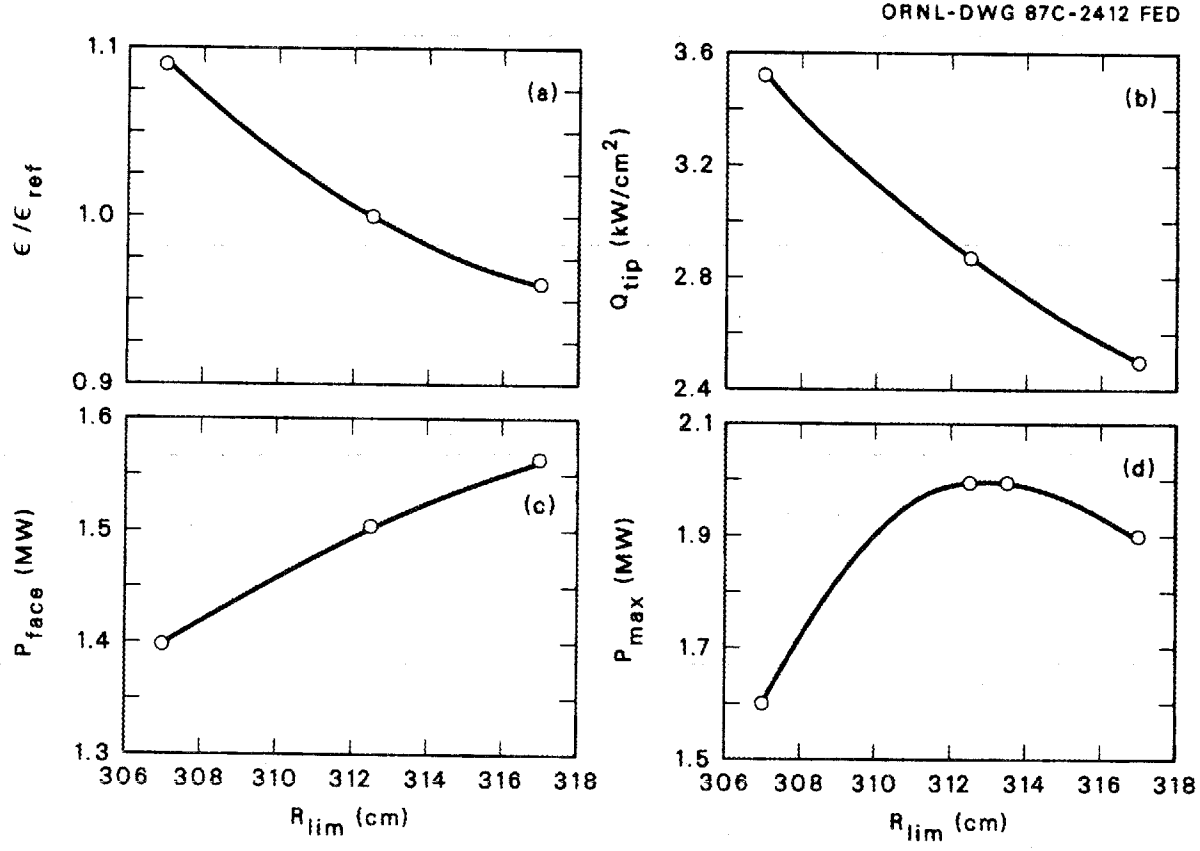

Fig. 8. Effects on limiter performance resulting from changes in limiter radius: (a) exhaust efficiency of the module, (b) heat flux at the leading edge, (c) heat removed by the front face, and (d) the upper limit of total power to be handled by the module.

the load on the front face of the limiter. If this heat load is to be maintained at the design level (~1.5 MW), the maximum power handled by the entire limiter must be reduced accordingly (Fig. 8d). The limit on total power is set by the load on the front face at the large radii. For smaller radii, the limit is determined by heat flux at the leading edge.

III.D. Application to RF Antennas

The shape proposed for the Tore Supra rf antennas (Fig. 9a) is much simpler than that of the limiter.[18] It is a line segment of 3.9° slope followed by a circular leading edge. The sloped, flat part is intended to follow approximately the shape of the field lines so that the electron density remains nearly constant over its toroidal extent. The circular leading edge protrudes radially a few millimeters into the plasma to protect the Faraday shield (flat part) from the plasma. The field lines shown in the figure are traced with the same five-loop magnetic field model. They are started at 0.3-cm intervals radially at $x = 0$.

Note that the leading edge does, in fact, protect most of the flat surface from direct contact with the plasma. At the only toroidal location where the plasma contacts the antenna, the surface is nearly parallel to the field lines. This should keep the normal component of the heat flux low. Figure 9b shows the heat flux at the leading edge, assuming an edge parallel heat flux of 10 kW/cm^2, which is consistent with modeling calculations.[7] The distances from the plasma edge are also plotted in Fig. 9b. The variation in these distances is small (~±2.5 mm). Because no plasma should be in the small scrape-off regions between the field line tangent to the antenna and the front surface of the antenna, this model shows no heat flux for these regions. In addition, if y_1 is the distance of the leading edge from the plasma edge, the distances $\Delta y - y_1$ are actually the distances between the Faraday shields and the location of the first plasma that the radiation from the antenna encounters.

IV. ANALYTICAL MODEL

Because of its inherent periodicity, the ripple is usually modeled as a cosine perturbation in the form

$$B_\Phi = \overline{B}_\Phi[1 - \delta(r,\theta)\cos N\Phi] \ , \tag{1}$$

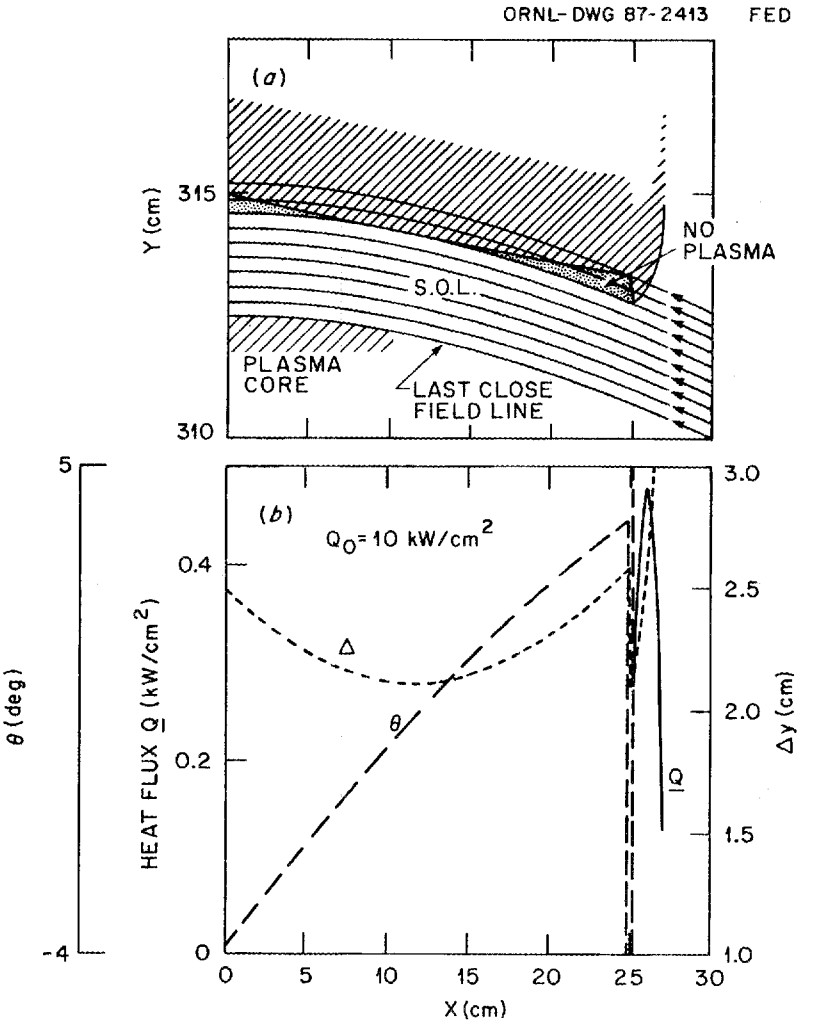

Fig. 9. Plots for the Tore Supra radio frequency antenna: (a) a graph showing the front surface of the head and edge field lines (x and y axes are drawn to different scales) and (b) a graph showing distances (Δy) between the front antenna surface and the plasma edge, the angle (θ) between the field lines and the surface, and the heat flux density (Q) on the surface that has been normalized so that the edge heat flux is 10 kW/cm^2.

where

$$\delta(r,\theta) = \frac{\Delta B_\Phi}{\overline{B}_\Phi} = \frac{B_\Phi^{\max} - B_\Phi^{\min}}{B_\Phi^{\max} + B_\Phi^{\min}} ,$$

$$B_\Phi^{\max} \equiv B_\Phi(r,\theta,\Phi = \Phi_m) , \quad B_\Phi^{\min} \equiv B_\Phi(r,\theta,\Phi = 0) , \quad \Phi_m = \pi/N_{\text{coil}} \quad \text{(Fig. 1)} ,$$

and (r,θ,Φ) are the toroidal coordinates.

Note that $\overline{B}_\Phi$ also has a poloidal dependence because of the finite aspect ratio (toroidal effect):

$$\overline{B}_\Phi = \frac{B_0 R_0}{R} = \frac{B_0 R_0}{R_0(1+\epsilon\cos\theta)} = \frac{B_0}{1+\epsilon\cos\theta} \equiv \frac{B_0}{h} ,$$

where $\epsilon = a/R_0$ is the inverse aspect ratio.

To first order in ϵ, δ, write

$$B_\Phi \approx B_0[1 - \epsilon\cos\theta - \delta(r,\theta)\cos N\Phi] . \tag{2}$$

The radial component of the field that results from this perturbation can then be derived from the requirement that $\vec{\nabla}\cdot\vec{B} = 0$ or

$$\frac{\partial}{\partial r}(rhB_r) + \frac{r}{R_0}\frac{\partial}{\partial\Phi}B_\Phi = 0 . \tag{3}$$

The remaining task is to find an appropriate model for $\delta(r,\theta)$. One such model is[5]

$$\delta(r,\theta) = \delta(r)\ g(\theta) = \delta_0\left(\frac{r}{a}\right)^m g(\theta) . \tag{4}$$

Combining Eqs. (2), (3), and (4) gives

$$\frac{\partial}{\partial r}(rhB_r) = -B_0\epsilon\ \delta_0\left(\frac{r}{a}\right)^{m+1} g(\theta)\ N\sin N\Phi ,$$

which when integrated becomes

$$B_r = \frac{B_0}{h}\frac{\epsilon}{m+2}\delta(r,\theta)\ N\sin N\Phi . \tag{5}$$

As in the case of the current loop simulation, the field lines can now be traced by using the field line equation

$$\frac{dr}{B_r} = \frac{R\ d\Phi}{B_\Phi} .$$

Radial displacements of the field line from its nonrippled path are obtained by integrating dr over the toroidal extent of interest

$$\delta r = \int_0^{\delta r} dr = \int_0^{\delta\Phi} R\frac{B_r}{B_\Phi} d\Phi \ .$$

If Eqs. (2) and (5) are used, this becomes

$$\delta r = \int_0^{\delta r} dr = \int_0^{\delta\Phi} R\frac{\epsilon\ \delta(r,\theta)}{m+2}\frac{N\sin N\Phi}{1-\delta(r,\theta)\cos N\Phi} d\Phi \ ,$$

which becomes

$$\delta r(r,\theta) = \frac{R\epsilon}{m+2}\ln\left[\frac{1-\delta(r,\theta)\cos N\Phi}{1-\delta(r,\theta)}\right] \ . \tag{6}$$

Values for m and δ are determined by fitting the results of magnetic field computations, such as those described earlier. For $r = 75$ cm, $\theta = 0°$, and $R_0 = 236$ cm, $\delta \approx 6\%$ and $m \approx 4.5$ best fit the data.

Figure 10 shows a comparison of a field line trace obtained from Eq. (6) with the CCD calculation.

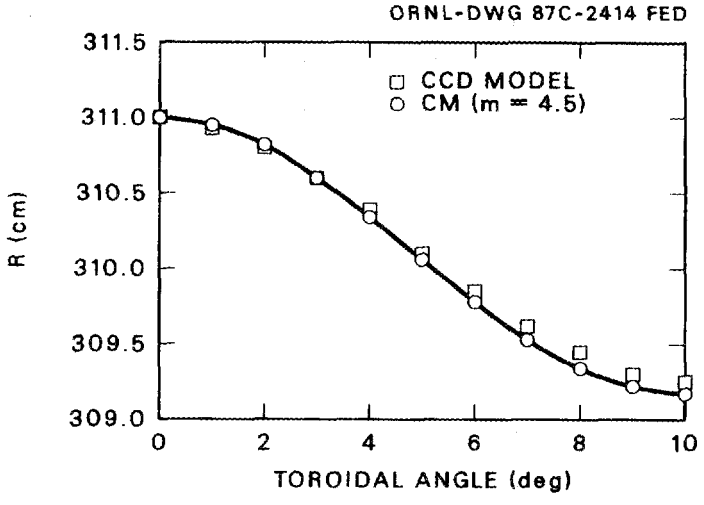

Fig. 10. Comparison of field lines traced by the analytical model [cosine model (CM)] and by the CCD calculation. The values of $\delta = 6$ and $m = 4.5$ are used in the CM calculation.

V. CONCLUSIONS

In Tore Supra, the amplitude of the ripple at the outboard edge is as much as 8%. This can cause up to a factor-of-2 increase in heat flux deposited onto the outboard limiter face. It also reduces the particle removal efficiency of the pump

limiters by increasing the distance of the throat opening from the plasma edge and by causing the neutralizer plate to be shadowed by the limiter head.

A simple, but accurate, scheme for field line tracing was found and used to study this effect. It involves representing the toroidal field coils by five current-carrying loops, whose location and share of the total coil current are optimized to match the results of computations using large numbers of loops. A better-than-10% agreement is achieved.

As a result of this study, a method was found for adjusting the shape of the limiter head, which was already optimized for particle and heat removal for a non-rippled edge magnetic flux. The resulting pump limiter was found to have heat and particle removal properties in the presence of the ripple that were almost identical to those of the original, unchanged limiter in the absence of ripple. It is then possible to design the limiters for future devices before the ripple, which is strongly dependent on the physical dimensions of the coils, is known. As soon as the coil design is known, the design can be corrected by using the described techniques.

Analytical modeling of the ripple is also discussed. This involves representing the edge field lines by a product of radial, poloidal, and toroidal functions. The last is a cosine function, and the radial dependence is a power of the radius. Both the amplitude of the cosine and the power are parameters that must be given. With values of these parameters obtained from fits of previously computed edge fields, it was shown that field lines can be traced very accurately by means of these analytical expressions.

ACKNOWLEDGMENTS

Valuable discussions with J. A. Rome, J. H. Harris, and G. H. Neilson of ORNL and M. Tuszewski of LANL are acknowledged. The technical assistance of R. H. Fowler and V. E. Lynch of the Computing and Telecommunications Division, Martin Marietta Energy Systems, Inc., is greatly appreciated.

REFERENCES

1. M. TUSZEWSKI and J. P. ROUBIN, "Fast Ion Ripple Losses During Neutral Injection in TFR," to be published in *Nuclear Fusion.*
2. S. D. SCOTT et al., "Measurement of Periodic Ripple Transport in ISX-B Tokamak," *Nucl. Fusion*, **25**, 359–82 (1985).
3. L. M. HIVELY, "TF-Ripple Losses from a Non-Circular Tokamak," *Nucl. Fusion*, **24**, 779–83 (1984).
4. T. TONE et al., "Effects of Toroidal Field Ripple on the Loss of Energetic Injected Particles and Toroidal Coil Configuration in a Tokamak Reactor," *J. Nucl. Sci. Technol.* **18**, 684–96 (1981).
5. N. A. UCKAN et al., "Toroidal Field Ripple Effects in Large Tokamaks," Proc. 8th Symp. Engineering Problems of Fusion Research, San Diego, California, November 18–21, 1975, p. 1105, Institute of Electrical and Electronics Engineers (1975) [also published as ORNL/TM-5603 (September 1976)].
6. P. DESCHAMPS et al., "Power Exhaust and Plasma-Surface Interaction Control in Tore Supra," *J. Nucl. Mater.*, **128&129**, 38 (1984).
7. T. UCKAN et al., "Modular Pump Limiter Systems for Large Tokamaks," ORNL/TM-10164, Oak Ridge National Laboratory (in preparation).
8. C. RUCHTI, *FLP: A Field Line Plotting Code for Bundle Divertor Design*, ORNL/TM-7555, Oak Ridge National Laboratory (January 1981).
9. L. M. HIVELY et al., "Constrained Ripple Optimization of Tokamak Bundle Divertors," *Nucl. Technol./Fusion* **2**, 372–91 (1982).
10. J. C. WHITSON and W. I. van RIJ, "Magnetic Field due to a Uniformly Wound Untwisted Flat Coil of Rectangular Cross-Section," *J. Appl. Phys.*, **47**(7), 3291–94 (July 1976).
11. C. GOURDON, *Programme de Calculs Numeriques dans une Configuration Magnetique Complex*, EUR-CEA-FC-413 (December 1966).
12. R. AYMAR, B. BAREYT, G. BON MARDION, et al., *Tore Supra—Basic Design Tokamak System*, EUR-CEA-CE-1068 (1980).
13. C. L. BARTBERGER, "The Magnetic Field of a Plane Circular Loop," *J. Appl. Phys.*, **21**, 1108 (November 1950).
14. R. H. FOWLER, Oak Ridge National Laboratory, "BDLOOP—A Program for the Calculation of the Magnetic Field and Its First Order Derivatives Due to a Set of Current Loops," Private Communication (August 20, 1986).

15. K. MIYAMOTO, *Plasma Physics for Nuclear Fusion*, MIT Press, Cambridge, Mass. (1980).
16. V. D. SHAFRANOV, *Reviews of Plasma Physics*, Vol. II, p. 124, Consultants Bureau, New York (1966).
17. J. B. WHITLEY et al., "Engineering Considerations for the Tore Supra Pump Limiter," *Proc. 14th Symp. Fusion Technology (SOFT)—Avignon, France (8–12 September 1986)*, Vol. 1, pp. 627–635, Pergamon Press, Oxford, Great Britain (1987).
18. F. W. BAITY, Oak Ridge National Laboratory, Private Communication (April 20, 1987).

ORNL/TM-10428
Dist. Category UC-421, 424, 426

INTERNAL DISTRIBUTION

1. L. A. Berry
2. R. A. Dory
3. J. L. Dunlap
4. J. H. Harris
5. D. L. Hillis
6. J. T. Hogan
7. R. C. Isler
8–12. C. C. Klepper
13. E. A. Lazarus
14. J. F. Lyon
15–19. P. K. Mioduszewski
20. O. B. Morgan
21. M. Murakami
22. G. H. Neilson
23. M. J. Saltmarsh
24. J. Sheffield
25. D. W. Swain
26. N. A. Uckan
27–31. T. Uckan
32–33. Laboratory Records Department
34. Laboratory Records, ORNL-RC
35. Document Reference Section
36. Central Research Library
37. Fusion Energy Division Library
38–39. Fusion Energy Division Publications Office
40. ORNL Patent Office

EXTERNAL DISTRIBUTION

41. R. T. McGrath, Sandia National Laboratories, Albuquerque, NM 87175
42. P. Hertout, Centre d'Etudes Nucléaires/Cadarache, F-13108 Saint Paul-lez-Durance Cedex, France
43. R. A. Blanken, Experimental Plasma Research Branch, Division of Applied Plasma Physics, Office of Fusion Energy, Office of Energy Research, ER-542, Germantown, U.S. Department of Energy, Washington, DC 20545
44. K. Bol, Princeton Plasma Physics Laboratory, P.O. Box 451, Princeton, NJ 08543
45. R. A. E. Bolton, IREQ Hydro-Quebec Research Institute, 1800 Montee Ste.-Julie, Varennes, P.Q. JOL 2P0, Canada
46. D. H. Crandall, Experimental Plasma Research Branch, Division of Applied Plasma Physics, Office of Fusion Energy, Office of Energy Research, ER-542, Germantown, U.S. Department of Energy, Washington, DC 20545
47. R. L. Freeman, GA Technologies, Inc., P.O. Box 85608, San Diego, CA 92138
48. K. W. Gentle, RLM 11.222, Institute for Fusion Studies, University of Texas, Austin, TX 78712
49. R. J. Goldston, Princeton Plasma Physics Laboratory, P.O. Box 451, Princeton, NJ 08543

50. J. C. Hosea, Princeton Plasma Physics Laboratory, P.O. Box 451, Princeton, NJ 08543
51. D. Markevich, Division of Confinement Systems, Office of Fusion Energy, Office of Energy Research, ER-55, Germantown, U.S. Department of Energy, Washington, DC 20545
52. R. H. McKnight, Experimental Plasma Research Branch, Division of Applied Plasma Physics, Office of Fusion Energy, Office of Energy Research, ER-542, Germantown, U.S. Department of Energy, Washington, DC 20545
53. E. Oktay, Division of Confinement Systems, Office of Fusion Energy, Office of Energy Research, ER-55, Germantown, U.S. Department of Energy, Washington, DC 20545
54. D. Overskei, GA Technologies, Inc., P.O. Box 85608, San Diego, CA 92138
55. R. R. Parker, Plasma Fusion Center, NW 16-288, Massachusetts Institute of Technology, Cambridge, MA 02139
56. W. L. Sadowski, Fusion Theory and Computer Services Branch, Division of Applied Plasma Physics, Office of Fusion Energy, Office of Energy Research, ER-541, Germantown, U.S. Department of Energy, Washington, DC 20545
57. J. W. Willis, Division of Confinement Systems, Office of Fusion Energy, Office of Energy Research, ER-55, Germantown, U.S. Department of Energy, Washington, DC 20545
58. A. P. Navarro, Division de Fusion, CIEMAT, Avenida Complutense 22, E-28040 Madrid, Spain
59. Laboratory for Plasma and Fusion Studies, Department of Nuclear Engineering, Seoul National University, Shinrim-dong, Gwanak-ku, Seoul 151, Korea
60. Office of the Assistant Manager for Energy Research and Development, U.S. Department of Energy, Oak Ridge Operations Office, P.O. Box E, Oak Ridge, TN 37831
61. J. D. Callen, Department of Nuclear Engineering, University of Wisconsin, Madison, WI 53706-1687
62. Dr. John F. Clarke, ,ssociate Director for Office of Fusion Energy, Office of Energy Research, ER-50 Germantown, U.S. Department of Energy, Washington, DC 20545
63. R. W. Conn, Department of Chemical, Nuclear, and Thermal Engineering, University of California, Los Angeles, CA 90024
64. S. O. Dean, Fusion Power Associates, Inc., 2 Professional Drive, Suite 248, Gaithersburg, MD 20879
65. H. K. Forsen, Bechtel Group, Inc., Research Engineering, P. O. Box 3965, San Francisco, CA 94119
66. J. R. Gilleland, L-644, Lawrence Livermore National Laboratory, P.O. Box 5511, Livermore, CA 94550
67. R. W. Gould, Department of Applied Physics, California Institute of Technology, Pasadena, CA 91125

68. R. A. Gross, Plasma Research Laboratory, Columbia University, New York, NY 10027
69. D. M. Meade, Princeton Plasma Physics Laboratory, P.O. Box 451, Princeton, NJ 08543
70. M. Roberts, International Programs, Office of Fusion Energy, Office of Energy Research, ER-52 Germantown, U.S. Department of Energy, Washington, DC 20545
71. W. M. Stacey, School of Nuclear Engineering and Health Physics, Georgia Institute of Technology, Atlanta, GA 30332
72. D. Steiner, Nuclear Engineering Department, NES Building, Tibbetts Avenue, Rensselaer Polytechnic Institute, Troy, NY 12181
73. R. Varma, Physical Research Laboratory, Navrangpura, Ahmedabad 380009, India
74. Bibliothek, Max-Planck Institut für Plasmaphysik, Boltzmannstrasse 2, D-8046 Garching, Federal Republic of Germany
75. Bibliothek, Institut für Plasmaphysik, KFA Jülich GmbH, Postfach 1913, D-5170 Jülich, Federal Republic of Germany
76. Bibliothek, KfK Karlsruhe GmbH, Postfach 3640, D-7500 Karlsruhe 1, Federal Republic of Germany
77. Bibliotheque, Centre de Recherches en Physique des Plasmas, Ecole Polytechnique Fédérale de Lausanne, 21 Avenue des Bains, CH-1007 Lausanne, Switzerland
78. R. Aymar, CEN/Cadarache, Departement de Recherches sur la Fusion Contrôlée, F-13108 Saint-Paul-lez-Durance Cedex, France
79. Bibliothèque, CEN/Cadarache, F-13108 Saint-Paul-lez-Durance Cedex, France
80. Library, Culham Laboratory, UKAEA, Abingdon, Oxfordshire, OX14 3DB, England
81. Library, JET Joint Undertaking, Abingdon, Oxfordshire OX14 3EA, England
82. Library, FOM-Instituut voor Plasmafysica, Rijnhuizen, Edisonbaan 14, 3439 MN Nieuwegein, The Netherlands
83. Library, Institute of Plasma Physics, Nagoya University, Chikusa-ku, Nagoya 464, Japan
84. Library, International Centre for Theoretical Physics, P.O. Box 586, I-34100 Trieste, Italy
85. Library, Centro Richerche Energia Frascati, C.P. 65, I-00044 Frascati (Roma), Italy
86. Library, Plasma Physics Laboratory, Kyoto University, Gokasho, Uji, Kyoto 611, Japan
87. Plasma Research Laboratory, Australian National University, P.O. Box 4, Canberra, A.C.T. 2601, Australia
88. Library, Japan Atomic Energy Research Institute, Naka Fusion Research Establishment, 801-1 Mukoyama, Naka-machi, Naka-gun, Ibaraki-ken, Japan

89–145. Given distribution as shown in OSTI-4500, Magnetic Fusion Energy (Category Distribution UC-421, 424, and 426)